

# SteerFace: Debiasing Synthetic Face Generation via Adaptive Residue Perturbation

Yuxi Mi  
yxmi20@fudan.edu.cn  
Fudan University  
Shanghai, China

Qiuyang Yuan  
qyyuan23@m.fudan.edu.cn  
Fudan University  
Shanghai, China

Jianqing Xu  
joejqxu@tencent.com  
Youtu Lab, Tencent  
Shanghai, China

Yichun Zhou  
yichunzhou25@m.fudan.edu.cn  
Fudan University  
Shanghai, China

Xuan Zhao  
xzha023@m.fudan.edu.cn  
Fudan University  
Shanghai, China

Jun Wang  
earljwang@tencent.com  
WeChat Pay Lab33, Tencent  
Shenzhen, China

Rizen Guo  
rizenguo@tencent.com  
WeChat Pay Lab33, Tencent  
Shenzhen, China

Shuigeng Zhou  
sgzhou@fudan.edu.cn  
Fudan University  
Shanghai, China

## Abstract

The shortage of legally compliant data for face recognition training has sparked growing interest in using synthetic data as an alternative. While recent diffusion-based methods enable the generation of photorealistic face images with strong identity adherence and data diversity, their downstream recognition performance still exhibits a significant synthetic-real gap. This paper identifies visual tendency as a previously underexplored limitation, whereby synthetic data exhibit an unrealistic prevalence of visual attributes and thus deviate from the real-data distribution. Visual tendency can be attributed to the generator’s conditioning on identity embeddings, through which co-occurring residual visual cues are unintentionally absorbed into learned identity semantics. To discourage the generator from exploiting such visual cues, this paper proposes SteerFace, a simple and efficient training framework that perturbs identity embeddings by steering them toward random orthogonal directions on the embedding hypersphere. The perturbation serves as an identity-preserving regularizer that penalizes the generator’s reliance on non-identity components, as supported by theoretical analysis. This paper further introduces an adaptive strategy that learns perturbation strengths with both sample-wise preference and favorable overall statistics. Extensive experiments show that SteerFace effectively mitigates visual tendency, outperforms prior methods in downstream face recognition, and generalizes well across different training datasets and generation pipelines.

## CCS Concepts

• Computing methodologies → Biometrics.

## Keywords

Face recognition, Face image synthesis, Diffusion model

## 1 Introduction

Face recognition (FR) is among the most prominent applications of computer vision. Its success relies on large-scale training datasets of face images from tens of thousands of individuals [8, 19, 25,

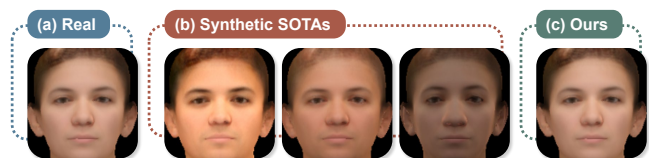


**Figure 1: Visual tendency in synthetic face generation, illustrated by 3DMM rendering of the dataset-wise average face. Compared with (a) real data, (b) synthetic SOTAs exhibit varying degrees of overall visual leaning, indicating a distribution bias. (c) SteerFace mitigates this bias.**

63]. However, the legitimate acquisition of face data remains a crucial challenge: most existing datasets were web-crawled without informed consent [34], which has raised ethical concerns and led to the withdrawal of several well-known datasets [8, 19]. This shortage of legally compliant data has sparked interest in synthetic data of “virtual” persons as alternatives for training FR models.

Ideally, synthetic data should mimic real data closely enough that FR models trained on them generalize effectively to real persons. Prior studies typically assess this goal through two proxy criteria: *identity adherence* [4, 27], which requires each synthetic image to faithfully preserve an assigned virtual identity; and *data diversity* [2, 31, 33, 37, 41], which requires the dataset as a whole to cover broad real-world variations. With recent advances in diffusion models (DMs) [21, 45, 49], state-of-the-art (SOTA) methods have made substantial progress on both criteria, generating photorealistic face images with strong identity consistency and rich variation. Nevertheless, their FR performance still exhibits a significant synthetic-real gap [9, 10]. This discrepancy suggests that the prevailing criteria, while important, may not fully capture the aspects of synthetic data quality that matter for FR.

To probe what may still be missing, this paper revisits synthetic data from a different dataset-level perspective. While data diversity measures the richness of variation, it remains unclear whether such variations appear with realistic prevalence. To examine this

point, given a dataset, this paper employs a 3D morphable model (3DMM) [14] to parameterize each face image by a set of visual attributes, including shape, expression, texture, and illumination. These attributes are averaged over the dataset and rendered into an “average face”, which represents the dataset’s overall visual tendency. Figure 1(a-b) compares the average face of a synthetic SOTA with that of real-world ground truth, and reveals a clear difference in, *e.g.*, color tone. This suggests that a synthetic dataset can be diverse yet still exhibit an overall visual leaning, yielding a *distribution bias* that weakens FR performance.

This paper traces the bias largely to how DMs learn identity adherence. As a *de facto* training practice, SOTAs pair each image with its identity embedding, commonly extracted via an off-the-shelf FR model, so that the DM learns to reproduce the image of the prescribed person. While such embeddings are identity-discriminative, prior studies have shown that they are also entangled with rich visual cues [12, 23, 61]. As a result, the DM may unintentionally absorb these cues as part of identity. Once learned in this way, the condition no longer specifies only who the person is, but also implicitly binds that identity to biased visual preferences.

To address this bias, this paper proposes a simple and efficient training scheme, *SteerFace*, which perturbs identity during training by geometrically steering it in the embedding space. The perturbation regularizes the DM’s reliance on co-occurring residual visual cues, as shown in Fig. 1(c). Importantly, unlike common regularization techniques such as context dropout [4, 22], it acts *selectively* on non-essential cues, thereby reducing distribution bias while better maintaining identity adherence. It also improves data diversity by allowing visual attributes to vary more freely, rather than being bound to identity. This paper further proposes an adaptive strategy that learns an improved sample-aware allocation of perturbation intensity. Experiments show that *SteerFace* is broadly effective across different training datasets and generation pipelines, and achieves superior downstream FR performance than all SOTAs.

Overall, this paper presents three main contributions:

- We identify biased visual tendency in identity-conditioned face generation as a major challenge for synthetic FR data.
- We propose *SteerFace*, which reduces this bias by geometrically and adaptively perturbing identity during training.
- We present extensive analyses showing that *SteerFace* outperforms SOTAs in both generation quality and downstream FR performance.

## 2 Related Work

### 2.1 Face Recognition

The success of modern FR is built on the progress of robust feature extractors [20], discriminative objectives [3, 12, 23, 26, 52], and large-scale training datasets [8, 19, 25, 63]. However, acquiring diverse and legally compliant datasets remains a crucial challenge [34], and ethical disputes have led to the withdrawal of several major datasets [8, 19]. This has sparked interest in using synthetic data as an alternative source for training FR models [9, 10].

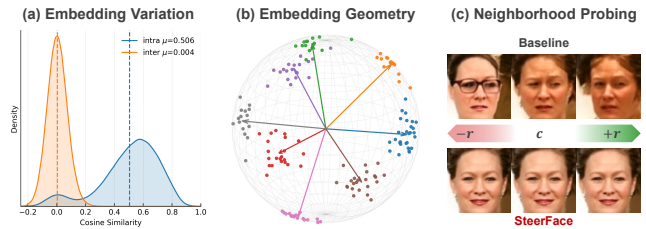


**Figure 2: Cause and effect of visual tendency.** (a) Embeddings exhibit image-wise variation due to co-occurring visual cues, reflected by widely varying intra-class similarity. (b) Geometrically, embeddings (marked ●) are distributed around the ideal identity (marked ↑) on the hypersphere. (c) Under local identity perturbation, a baseline generator changes appearance due to entangled visual cues; *SteerFace* largely preserves appearance, indicating mitigated visual tendency.

### 2.2 Face Image Synthesis

Generating high-quality face images is a long-standing challenge. Early works primarily employ 3D graphics [11, 17, 43, 55] or generative adversarial networks (GANs) [24, 35, 39]. The recent rise of DMs [21, 45, 49] has further enabled photorealistic face generation and plausible personalization to specific subjects by conditioning the DM on reference images [13, 15, 47], identity-descriptive features [32, 42, 51, 53, 54, 57], or textual prompt [16, 62] of the person. Though these methods have shown success in tasks such as entertainment [18, 60] and privacy preservation [36, 61], they are not readily suitable for FR training, due to insufficient identity retention [4] and limited diversity in generation at scale [9].

### 2.3 Face Synthesis for Recognition

Synthetic data for FR training requires *scalable* generation of face images that each accurately adhere to virtual identities and together exhibit rich variation that mimics the diversity of faces in the wild. To retain identity, early GAN-based works such as *SynFace* [44] manipulate the identity latent space; *SFace* [6], *SFace2* [5], *IDNet* [29], and *ExFaceGAN* [7] adopt *StyleGAN* [24] for identity-conditioned generation. Among DM-based methods, *IDiff-Face* [4] conditions DM on identity embeddings extracted from a pretrained FR model, which has since become a *de facto* practice. To enrich diversity, *DigiFace* [1] utilizes 3D priors to produce distinctive yet less realistic faces, *IDiff-Face* [4] and *UIFace* [33] partially unconstrain identity conditions, *DCFace* [27] uses feature banks from auxiliary images, *Arc2Face* [41] inherits the knowledge of pre-trained *Stable Diffusion* [45], *CemiFace* [50] mines semi-hard samples, *ID3* [31] injects explicit facial attributes, *MorphFace* [37] uses 3DMM renderings as contexts, and *IDPerturb* [2] employs inference-time perturbations on identity conditions. While these works successfully improve data diversity, their generation commonly exhibits a distribution bias in visual tendency from real data, which hinders FR performance. Addressing this bias is the primary goal of this paper.

### 3 Methodology

#### 3.1 Preliminary

Latent diffusion model (LDM) [45] allows the generation of photo-realistic face images. It is trained under the DDPM [21] framework to predict the noise added to a latent code  $\mathbf{z} \in \mathbb{R}^{c \times h \times w}$ . Given an input image  $\mathbf{x} \in \mathbb{R}^{C \times H \times W}$ , it is mapped into the latent code via a pre-trained encoder  $\phi_e$  as  $\mathbf{z} = \phi_e(\mathbf{x})$ , and is then perturbed by Gaussian noise  $\epsilon \sim \mathcal{N}(0, 1)$  over  $T$  discrete steps,

$$\mathbf{z}_t = \sqrt{\alpha_t} \mathbf{z}_0 + \sqrt{1 - \alpha_t} \epsilon, \quad (1)$$

where  $\mathbf{z}_0$  denotes the clean latent code,  $\alpha_t$  is derived from a linearly scheduled variance term, and  $\bar{\alpha}_t = \prod_{i=1}^t \alpha_i$ . In the denoising process, the model predicts the noise via an estimator  $\epsilon_\theta$  (e.g., a U-Net [46]) and parameterizes the reverse transition from  $\mathbf{z}_t$  to  $\mathbf{z}_{t-1}$ ,

$$\mathbf{z}_{t-1} = \frac{1}{\sqrt{\alpha_t}} \left( \mathbf{z}_t - \frac{1 - \alpha_t}{\sqrt{1 - \bar{\alpha}_t}} \epsilon_\theta(\mathbf{z}_t, t, \mathbf{c}) \right) + \sqrt{1 - \alpha_t} \boldsymbol{\eta}, \quad (2)$$

where  $\boldsymbol{\eta} \sim \mathcal{N}(0, 1)$ .  $\mathbf{z}_0$  is decoded into the image space as  $\mathbf{x} = \phi_d(\mathbf{z}_0)$ .  $\mathbf{c} \in \mathbb{R}^d$  is a context embedding that conditions the recovery, injected into the noise estimator through cross-attention. We hereafter omit the latent encoding  $\mathbf{x} \mapsto \mathbf{z}$  for notional simplicity.

#### 3.2 Visual Tendency in Synthetic Data

We begin by explaining why synthetic data can exhibit visual tendency. The general goal of synthetic face generation for FR is to create a scalable set of real-looking face images  $\mathbf{X} = \{\mathbf{x}_1, \dots, \mathbf{x}_n\}$  that adhere to many virtual identities  $V = \{v_1, \dots, v_m\}$ , thereby serving as an alternative for FR training. A common paradigm in recent studies [2, 4, 27, 31, 33, 37] is to train an LDM generator  $\mathcal{G}$  on legally compliant real data (e.g., CASIA [56]). Identity adherence is encouraged by training the generator to reconstruct a face image  $\mathbf{x}$  conditioned on its identity embedding  $\mathbf{c}$  (i.e.,  $\mathcal{G} : (\mathbf{x}, \mathbf{c}) \mapsto \mathbf{x}$ ), as,

$$\mathcal{L}_{\text{LDM}} = \mathbb{E}_{\mathbf{x}, t, \epsilon} [\|\epsilon_\theta(\mathbf{x}_t, t, \mathbf{c}) - \epsilon\|_2^2], \quad 0 < t \leq T. \quad (3)$$

Ideally, the generator would learn from a “pure” embedding  $\mathbf{c}_v$  that encodes only identity. However, such an embedding is hard to obtain, as face images do not present identity in isolation. In practice, SOTAs use embeddings extracted via an off-the-shelf FR model  $\mathbf{c} = \mathcal{F}(\mathbf{x})$ , which are identity-discriminative unit vectors by design. This is a compromise, as such embeddings also retain information about co-occurring visual attributes entangled in a particular image [12, 52], e.g., shape, expression, texture, and illumination, thus exhibiting image-wise variation. Figure 2(a) shows the pairwise intra-class similarity of embeddings from CASIA [56], which spans a fairly wide range rather than collapsing to a single value. Geometrically, embeddings from different images of the same person form a local neighborhood on an  $\mathbb{S}^{d-1}$  unit hypersphere around the hypothetical pure identity  $\mathbf{c}_v$ , as shown in Fig. 2(b). Formally, we can write  $\mathbf{c}$  as the composition of  $\mathbf{c}_v$  and a residual term  $\mathbf{r}$ :

$$\mathbf{c} = \text{norm}(\mathbf{c}_v + \mathbf{r}), \quad \mathbf{r} \perp \mathbf{c}_v. \quad (4)$$

Importantly, the residue is problematic for identity-conditioned generation. During training, any component of  $\mathbf{c}$  that is predictive of the target face appearance, whether identity-related or not, can help

minimize the reconstruction objective. In particular, conditioning on  $\mathbf{r}$  in addition to  $\mathbf{c}_v$  cannot make the optimal reconstruction worse:

$$\min_{\theta} \mathbb{E} [\|\epsilon_\theta(\mathbf{x}_t, t, \mathbf{c}_v) - \epsilon\|_2^2] \geq \min_{\theta} \mathbb{E} [\|\epsilon_\theta(\mathbf{x}_t, t, \mathbf{c}_v, \mathbf{r}) - \epsilon\|_2^2], \quad (5)$$

with strict improvement whenever  $\mathbf{r}$  is predictive of the denoising target. The generator is therefore encouraged to exploit not only identity but also the visual cues carried by the residue as short-cuts for reconstruction. In this process, it learns a biased coupling between identity and visual cues.

At inference, the trained generator synthesizes new faces  $\mathbf{x}'$  from Gaussian noise and a virtual identity embedding  $\mathbf{c}'$ , obtained either from a prior distribution [31] or from the reference image of a virtual person [4, 33, 37], i.e.,  $\mathcal{G} : (\mathcal{N}(0, 1), \mathbf{c}') \mapsto \mathbf{x}'$ . Under an ideal training outcome, the embedding should control only identity, while visual attributes vary freely according to the overall learned data distribution. However, the induced coupling causes the generator to also rely on the residue in  $\mathbf{c}'$ , thereby giving rise to certain visual tendency. To illustrate this effect, we fix the Gaussian noise and condition a SOTA generator [4] on a specific  $\mathbf{c}'$ , then perturb  $\mathbf{c}'$  within its local neighborhood to mimic residual variation. As shown in Fig. 2(c), this yields images of the same person with noticeable appearance changes, suggesting that the generator absorbs not only identity but also visual cues from  $\mathbf{c}'$ . Visual tendency has two adverse effects: it limits data diversity and, more importantly, introduces a distribution bias from real data.

#### 3.3 Geometric Residue Perturbation

To mitigate visual tendency, we introduce *SteerFace*, a simple and efficient generator training paradigm that discourages the learning of residue. Figure 3 shows its overall pipeline.

Our motivation stems from how the generator exploits the residue. We have shown in Eq. (5) that the generator uses the residue as a shortcut when it is predictive for denoising, which happens because the residue is deterministically coupled with its source image and thus carries stable visual cues, as shown in Fig. 4(a). By contrast, consider an *unpredictive* residue  $\hat{\mathbf{r}}$ , i.e., noise-like and (approximately) conditionally independent of the denoising target,

$$\epsilon \perp \hat{\mathbf{r}} \mid (\mathbf{x}_t, t, \mathbf{c}_v), \quad \mathbb{E}[\epsilon \mid \mathbf{x}_t, t, \mathbf{c}_v, \hat{\mathbf{r}}] = \mathbb{E}[\epsilon \mid \mathbf{x}_t, t, \mathbf{c}_v]. \quad (6)$$

It then offers no gain for the  $\mathcal{L}_{\text{LDM}}$  objective, hence no incentive for the generator to rely on it. This motivates mitigating visual tendency by perturbing the deterministic residue  $\mathbf{r}$  into a noise-like  $\hat{\mathbf{r}}$  that changes at each visit, thereby destroying its predictability.

Crucially, to maintain identity adherence, such perturbation should act on the residue  $\mathbf{r}$  while preserving the identity component associated with  $\mathbf{c}_v$ . Geometrically, this corresponds to adding an identity-orthogonal random noisy component  $\mathbf{n} \perp \mathbf{c}_v$  to the embedding  $\mathbf{c}$ , yielding  $\hat{\mathbf{c}} = \text{norm}(\mathbf{c} + \mathbf{n})$ ; thus, the residue is effectively corrupted as  $\hat{\mathbf{r}} = \mathbf{r} + \mathbf{n}$  before normalization. Since the pure  $\mathbf{c}_v$  is unavailable in practice, we instead use the good approximation that  $\mathbf{c}_v$  is angularly close to  $\mathbf{c}$ , i.e.,  $\langle \mathbf{c}_v, \mathbf{c} \rangle \approx 1$ , and choose  $\mathbf{n} \perp \mathbf{c}$  accordingly. We further discuss the validity of this approximation in the supplementary material.

We instantiate the perturbation by rotating the embedding toward a random orthogonal direction on the unit hypersphere  $\mathbb{S}^{d-1}$ .

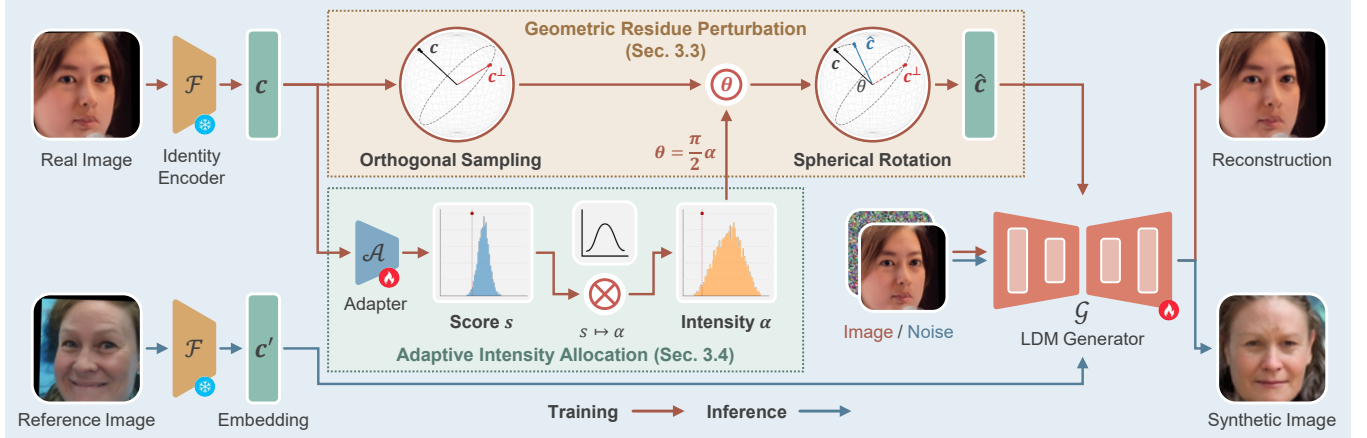


**Figure 3: Pipeline of SteerFace.** To mitigate visual tendency in synthetic face generation, during training, we perturb the identity embedding so that the generator is discouraged from exploiting visual cues. The perturbation is instantiated by spherically rotating the embedding toward a random orthogonal direction. The perturbation intensity is adaptively allocated to be both statistically favorable and sample-aware; further see Fig. 5. At inference time, generation follows the standard pipeline:  $\mathcal{G} : (\mathcal{N}(0, 1), c') \mapsto x'$ .

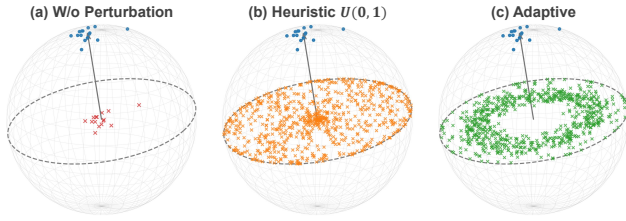


**Figure 4: Effect of SteerFace.** We experimentally sample one CASIA identity, revisit each of its embedding (marked  $\bullet$ ) 50 times, and plot the resulting residues ( $\times$ ). (a) Without perturbation, residues are mapped to a deterministic location on the plane orthogonal to ideal identity ( $\uparrow$ ), making them predictive and easy for the generator to exploit. (b) Heuristic perturbation turns residues into noise-like variations that spread across the plane at each visit, thereby regularizing generator learning. (c) Adaptive perturbation learns a spread with comparable identity retention but more favorable regularization, leading to better downstream FR performance.

Concretely, each time a training face sample  $x$  is visited, we extract its embedding  $c$  and isotropically sample a unit vector  $c^\perp \perp c$  by

$$c^\perp = \text{norm}(e - (c \cdot e)c), \quad e \sim \mathcal{N}(0, 1). \quad (7)$$

Then, we rotate  $c$  toward  $c^\perp$  by an angle  $\theta \in [0, \frac{\pi}{2})$ . To enhance the unpredictability of the noisy residue, we introduce perturbations with varying intensities by sampling a different  $\theta$  each time, parameterized as  $\theta = \frac{\pi}{2}\alpha$ , where  $\alpha$  follows a prior distribution, e.g.,  $\alpha \sim U(0, 1)$ . We use  $U(0, 1)$  as a heuristic baseline, and revisit its extension later in Sec. 3.4. The rotation is given by

$$\hat{c} = \cos \theta c + \sin \theta c^\perp. \quad (8)$$

From Eq. (8), the perturbed embedding is naturally decomposed into two parts: an identity component  $\cos \theta c$  and a noisy component

$\sin \theta c^\perp$ , where the latter serves as  $n$ . The generator is trained on perturbed embeddings as  $\mathcal{G} : (x, \hat{c}) \mapsto x$ . At inference time, as the generator has learned to suppress residue cues, perturbation is no longer applied, and generation follows the standard conditional pipeline:  $\mathcal{G} : (\mathcal{N}(0, 1), c') \mapsto x'$ .

We show that such residue perturbation is both *identity-preserving* and *residue-regularizing*: During training, for embeddings  $\{c_1, \dots, c_n\}$  of the same person, under the approximation  $\langle c_v, c \rangle \approx 1$ , the identity-bearing direction of each perturbed embedding remains aligned with  $c_v$ , scaled only by  $\cos \theta$ . Since FR embeddings encode identity primarily through angular direction [12], this preserves the overall identity structure while only mildly attenuating its training influence through scale. Meanwhile, their noisy components spread within the plane orthogonal to  $c_v$ , as shown in Fig. 4(b), making the residue noise-like and less exploitable by the generator.

To validate the debiasing effect, we retrain the same SOTA generator [4] from Sec. 3.2 on perturbed embeddings instead, and repeat the local-neighborhood probing. In Fig. 2(c), images of the same person remain largely unchanged despite residual variation, indicating that the generator has learned to disentangle identity from visual cues, thereby mitigating visual tendency. Results in Tab. 2 further show a 1.37% FR accuracy gain with  $U(0, 1)$  perturbation, suggesting that it improves downstream FR significantly.

Formally, we show that the perturbation serves as an implicit regularizer for identity-conditioned generation:

**THEOREM 1.** *Minimizing the  $\mathcal{L}_{\text{LDM}}$  objective with perturbed embeddings  $\hat{c}$  defined in Eqs. (7) and (8) penalizes the generator’s sensitivity to non-identity components. Regularization strength scales with  $\mathbb{E}[\sin^2 \theta]$  and expected identity retention is given by  $\mathbb{E}[\cos \theta]$ .*

The proof is deferred to the supplementary material.

We distinguish SteerFace from two related lines of work: *Context dropout* [4, 22] regularizes LDM conditioning by suppressing all semantics indiscriminately, whereas SteerFace preserves identity in a structured way. Several SOTAs [2, 31, 50] have explored

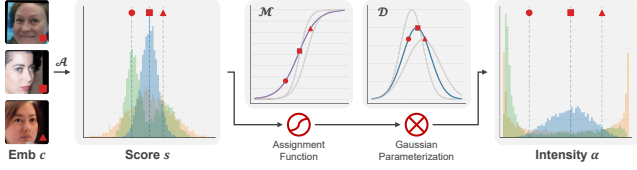


**Figure 5: Adaptive intensity allocation.** A score  $s$  of perturbation preference is assigned by adapter  $\mathcal{A}$ , and mapped to the final intensity  $\alpha$  through assignment function  $\mathcal{M}$  and Gaussian parameterization  $\mathcal{D}$ . The plots are experimentally derived. Notably, 1)  $\mathcal{D}$  is adaptively parameterized; 2) the adapter can learn diverse score distributions, which, when composed with  $\mathcal{M}$ , induce expressive intensity allocations (in different colors); and 3) within the same distribution, score and intensity preserve monotonic order ( $\bullet < \blacksquare < \blacktriangle$ ).

*inference-time perturbation* to enrich data diversity. IDPerturb [2] is particularly related to ours in that it also exploits spherical rotation. By contrast, SteerFace applies perturbation during training to align synthetic and real data distributions. See Sec. 4.6 for discussion.

### 3.4 Adaptive Intensity Allocation

We further investigate the allocation of perturbation intensity. Though the heuristic choice  $\alpha \sim U(0, 1)$  is empirically effective, it is neither *statistically optimal* nor *sample-aware*.

From a statistical perspective, Thm. 1 shows that the regularizing effect of perturbation becomes stronger as  $\mathbb{E}[\sin^2 \theta]$  increases, yet at the cost of weakening identity retention, as the identity component  $c_v$  is attenuated by  $\mathbb{E}[\cos \theta]$ . In balancing the two, we compare different heuristic distributions later in Tab. 2, and find that downstream FR generally favors stronger regularization. Meanwhile, prior studies [27, 33, 37] suggest that identity adherence need only be sufficient for the FR model to learn stable identity discrimination. This implies that, compared with  $U(0, 1)$ , a distribution that preserves adequate identity retention while inducing stronger regularization may be more favorable for downstream FR. On the other hand, sampling  $\alpha$  from  $U(0, 1)$  also falls short in perturbing all embeddings indiscriminately. In practice, embeddings differ in how strongly they are coupled with visual cues, and may therefore require different perturbation strengths.

To improve FR performance, we first seek an allocation of  $\alpha$  whose overall statistics are more favorable than those of  $U(0, 1)$ . However, directly learning a generic distribution is non-trivial, since the global constraints on identity retention and regularization are difficult to impose tractably. To simplify learning, we parameterize the allocation with a Gaussian family  $\mathcal{N}(\mu, \sigma)$ , whose overall shape can be controlled by only two parameters,  $\mu$  and  $\sigma$ , under explicit constraints. Despite its simplicity, this parameterization remains sufficiently expressive in the final distribution shape when combined with the sample-aware assignment introduced next.

Concretely, recall that the rotation angle is determined by the perturbation intensity as  $\theta = \frac{\pi}{2} \alpha$ . We parameterize the intensity as  $\alpha = \mathcal{D}(z) = \mu + \sigma z$ , where  $z$  denotes a sample-wise coordinate to be assigned later. We then regularize the induced  $\theta$  through two indicator statistics of identity retention and regularization, namely,

$\mathbb{E}[\cos \theta]$  and  $\mathbb{E}[\sin^2 \theta]$ . For identity retention, we want the learned allocation to remain comparable to  $U(0, 1)$ . We therefore regularize  $\mathbb{E}[\cos \theta]$  through the following consistency objective,

$$\mathcal{L}_{\text{id}} = \left( \mathbb{E}[\cos \theta] - \mathbb{E}_{\alpha \sim U(0,1)} \left[ \cos \left( \frac{\pi}{2} \alpha \right) \right] \right)^2. \quad (9)$$

Meanwhile, to encourage stronger regularization, we impose a soft encouragement term that favors larger  $\mathbb{E}[\sin^2 \theta]$ ,

$$\mathcal{L}_{\text{reg}} = \frac{1}{1 + k \mathbb{E}[\sin^2 \theta]}, \quad (10)$$

where  $k$  is a scaling coefficient, empirically set to 10. To improve upon  $U(0, 1)$  rather than learn from scratch, we further initialize  $\mu$  and  $\sigma$  to match that of  $U(0, 1)$ , namely,  $\mu_0 = \frac{1}{2}$ ,  $\sigma_0 = \sqrt{1/12}$ .

To enable sample-wise adaptation, we further train a lightweight MLP adapter  $\mathcal{A} : c \mapsto s$  jointly with the generator, which assigns each embedding  $c$  a scalar score  $s \in \mathbb{R}$ . The score indicates where the current embedding should be placed among all samples in terms of perturbation preference. To associate this score with the Gaussian family, we project it to a sample-wise coordinate through an assignment function  $\mathcal{M}$ . The function is monotonic, so that embeddings with stronger perturbation preference receive larger intensities, and nonlinear, so as to improve the expressiveness of the resulting allocation; see the supplementary material for details. The overall mapping from  $c$  to  $\alpha$  is thus given by

$$\alpha = (\mathcal{D} \circ \mathcal{M} \circ \mathcal{A})(c). \quad (11)$$

Notably, though  $\mathcal{D}$  itself follows a simple Gaussian parameterization, its composition with the adapter  $\mathcal{A}$  and the nonlinear assignment  $\mathcal{M}$  yields a sufficiently flexible allocation of  $\alpha$ , as illustrated in Fig. 5 and later experimentally shown in Fig. 8(b).

Combining the above with Eq. (3) yields the overall training objective of SteerFace under adaptive intensity allocation,

$$\mathcal{L} = \mathcal{L}_{\text{LDM}} + w_{\text{id}} \mathcal{L}_{\text{id}} + w_{\text{reg}} \mathcal{L}_{\text{reg}} + \mathcal{R}(\alpha), \quad (12)$$

where  $w_{\text{id}}$  and  $w_{\text{reg}}$  are weighting hyper-parameters.  $\mathcal{R}(\alpha)$  is a simple regularization term that prevents the dispersion of  $\alpha$  from collapsing; see the supplementary material for details. Figure 4(c) demonstrates the effect of adaptive allocation, where a more favorable distribution of perturbation intensity is learned in terms of identity retention and regularization. Table 2 further shows that it improves downstream FR by 0.51% over the heuristic  $U(0, 1)$ , and by 1.88% over training without perturbation.

## 4 Experiments

### 4.1 Experimental Setup

**4.1.1 Generator.** We instantiate the generator  $\mathcal{G}$  based on the open-source code of IDiff-Face [4], and train it on CASIA-WebFace [56]. The dataset contains 490K face images from 10,575 identities with varying image quality. We use an off-the-shelf ElasticFace [3] identity extractor  $\mathcal{F}$ , and the encoder  $\phi_e$  and decoder  $\phi_d$  from Stable Diffusion [45]. We train  $\mathcal{G}$  for 250K steps using the Adam optimizer [28], with an initial learning rate of  $10^{-4}$  and a total batch size of 512. We set  $w_{\text{id}} = 10$ ,  $w_{\text{reg}} = 1$ , and  $k = 10$ .

**Table 1: Comparison with SOTAs in terms of downstream FR accuracy. Results marked with an asterisk (\*) are our reproductions. Bold and underlined numbers indicate the best and second-best results, respectively; the same applies hereafter.**

Method	Venue	Generator	Scale (#IDs × #Imgs)	LFW	CFP-FP	AgeDB	CPLFW	CALFW	Average
CASIA [56]	(Real)	/	0.49M (10.5K × 47)	99.38	96.91	94.50	89.78	93.35	94.78
SynFace [44]	ICCV 21	GAN	0.5M (10K × 50)	91.93	75.03	61.63	70.43	74.73	74.75
SFace [6]	IJCB 22	GAN	0.6M (10K × 60)	91.87	73.86	71.68	77.93	73.20	77.71
DigiFace [1]	WACV 23	Rendering	0.5M (10K × 50)	95.40	87.40	76.97	78.87	78.62	83.45
IDNet [29]	CVPR 23	GAN	0.5M (10K × 50)	84.83	70.43	63.58	67.35	71.50	71.54
DCFace [27]	CVPR 23	DM	0.5M (10K × 50)	98.55	85.33	89.70	82.62	91.60	89.56
IDiff-Face [4]	ICCV 23	DM	0.5M (10K × 50)	98.00	85.47	86.43	80.45	90.65	88.20
ExFaceGAN [7]	IJCB 23	GAN	0.5M (10K × 50)	93.50	73.84	78.92	71.60	82.98	80.17
SFace2 [5]	BIOM 24	GAN	0.6M (10K × 60)	94.62	76.24	74.37	81.57	72.18	79.80
Arc2Face [41]	ECCV 24	DM	0.5M (10K × 50)	98.81	91.87	90.18	85.16	92.63	91.73
ID3 [31]	NeurIPS 24	DM	0.5M (10K × 50)	97.68	86.84	91.00	82.77	90.73	89.80
CemiFace [50]	NeurIPS 24	DM	0.5M (10K × 50)	99.03	91.06	91.33	87.65	92.42	92.30
UIFace [33]	ICLR 25	DM	0.5M (10K × 50)	<u>99.27</u>	<u>94.29</u>	90.95	<b>89.58</b>	92.25	93.27
MorphFace [37]	CVPR 25	DM	0.5M (10K × 50)	99.25	94.11	<u>91.80</u>	88.73	<u>92.73</u>	<u>93.32</u>
IDPerturb [2] *	CVPR 26	DM	0.5M (10K × 50)	99.08	93.50	<u>90.28</u>	87.93	91.87	92.53
<b>SteerFace</b>	(Ours)	DM	0.5M (10K × 50)	<b>99.40</b>	<b>94.67</b>	<b>92.73</b>	<b>88.85</b>	<b>92.95</b>	<b>93.72</b>
DigiFace [1]	WACV 23	Rendering	1.2M (10K × 72, 100K × 5)	96.17	89.81	81.10	82.23	82.55	86.37
DCFace [27]	CVPR 23	DM	1.2M (20K × 50, 40K × 5)	98.58	88.61	90.07	85.07	92.82	91.03
Arc2Face [41]	ECCV 24	DM	1.2M (20K × 50, 40K × 5)	98.92	94.58	92.45	86.45	93.33	93.15
UIFace [33] *	ICLR 25	DM	1.2M (10K × 50)	<u>99.27</u>	<u>95.13</u>	92.51	<u>90.63</u>	93.17	94.14
MorphFace [37]	CVPR 25	DM	1.2M (24K × 50)	<b>99.35</b>	94.77	<b>93.27</b>	90.07	<u>93.40</u>	<u>94.17</u>
IDPerturb [2] *	CVPR 26	DM	1.2M (24K × 50)	99.33	94.92	92.16	89.27	92.92	93.72
<b>SteerFace</b>	(Ours)	DM	1.2M (24K × 50)	<b>99.35</b>	<b>95.27</b>	<u>93.12</u>	<b>90.66</b>	<b>93.43</b>	<b>94.37</b>

**Figure 6: Generations and average faces of SteerFace and SOTAs. (a) Synthetic samples from two virtual subjects. (b) 3DMM renderings of dataset-wise average faces. Numbers in the corner indicate the synthetic-real distribution gap measured by MSE, where lower is better. SteerFace achieves the smallest gap among all SOTAs.**

**4.1.2 Synthetic face generation.** We use the virtual identity set  $V$  of 10K/24K reference face images publicly released by UIFace [33], which are generated by an unconditional DM [27]. For each identity, we synthesize 50 images at a resolution of  $128^2$ , yielding two synthetic datasets of 0.5M/1.2M images, respectively.

**4.1.3 Downstream FR.** We adopt IR-50 [20] as the downstream FR model. It takes synthetic images resized to  $112^2$  as input, and is trained for 32 epochs using the ArcFace [12] loss, with a batch size of 256 and a learning rate of 0.1, factored by 10 at epochs 22 and 28. We evaluate the trained model on 5 widely used benchmarks: LFW [30], CFP-FP [48], AgeDB [38], CPLFW [58], and CALFW [59].

## 4.2 Comparison with SOTAs

**4.2.1 FR performance.** We compare SteerFace with a real-data baseline, namely training on CASIA [56], as well as with 14 SOTAs: SynFace [44], SFace [6], DigiFace [1], IDNet [29], DCFace [27], IDiff-Face [4], ExFaceGAN [7], SFace2 [5], Arc2Face [41], ID3 [31], CemiFace [50], UIFace [33], MorphFace [37], and IDPerturb [2]. See Sec. 2.3 for their discussion. Notably, IDPerturb is by default instantiated from UIFace and thus enjoys a more favorable setting. Here we isolate its standalone effect, while evaluating their integration later in Tab. 3. Results are presented in Tab. 1.

We observe that SteerFace outperforms all SOTAs on most benchmarks as well as on average. It surpasses the best SOTA by 0.4/0.2% on average at the 0.5M/1.2M scales, and by 0.38% and 0.97% on CFP-FP and AgeDB, respectively. It also reduces the synthetic-real gap to 1.08%. Moreover, SteerFace at 0.5M already surpasses most SOTAs at 1.2M, demonstrating its strong effectiveness.

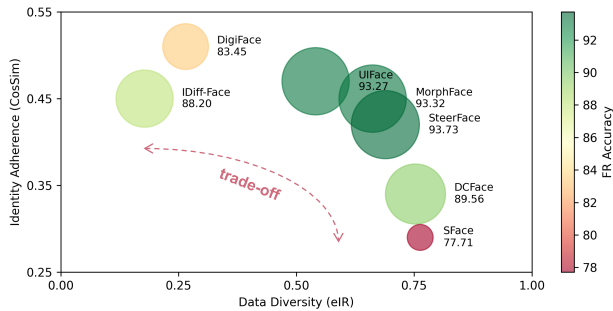


**Figure 7: Comparison of SteerFace and SOTAs in terms of identity adherence and data diversity. Circle color and size indicate downstream FR accuracy. SteerFace achieves a favorable balance and delivers superior FR performance.**

**4.2.2 Visualization.** We visualize samples from SOTAs with publicly available datasets, and compare them with CASIA and SteerFace in Fig. 6(a). We observe that SFace and DigiFace, as earlier GAN- or rendering-based methods, fall short in either identity retention or photorealism. IDiff-Face is among the foundational works that established identity adherence in DM-based generation, but shows limited diversity, with samples from the same identity appearing nearly duplicated. Later methods improve diversity, yet still exhibit noticeable visual tendency: DCFace generates a large proportion of smiling faces, while UIFace and MorphFace show unrealistic color tones. By contrast, SteerFace produces samples that are both diverse and more visually unbiased. Further see Sec. 4.3.

### 4.3 Synthetic Data Quality

We evaluate synthetic data quality by how closely it mimics real data, based on three criteria: *identity adherence*, *data diversity*, and, as newly focused in this work, overall *visual tendency*.

**4.3.1 Identity adherence vs. Data diversity.** Quantitatively, we measure identity adherence using the cosine similarity  $\langle c_1, c_2 \rangle$  between intra-person embeddings extracted by an off-the-shelf FR model [3], where higher similarity indicates stronger adherence. For diversity, we use extended improved recall (eIR) [27], which measures the sparsity of the style-feature manifold, with larger values indicating better diversity. Figure 7 plots prior SOTAs and SteerFace in the similarity-eIR space. Overall, a clear trade-off is observed, with most SOTAs favoring either adherence or diversity. SteerFace lies near the top-right frontier, indicating a better balance between the two. In particular, SteerFace is implemented based on IDiff-Face yet achieves substantially higher diversity. While SteerFace does not explicitly encourage diversity, it promotes it naturally by mitigating visual tendency, thereby allowing generation to vary more freely across the overall data distribution.

**4.3.2 Visual tendency.** Visual tendency reflects bias in the data distribution. For each SOTA, we use the same 3DMM [14] as in Fig. 1 to extract the dataset-level average of visual attributes and render it into an “average face”. The results are shown in Fig. 6(b), with the mean squared error (MSE) to the real-world ground truth marked in the corner. We observe that all SOTAs exhibit visual tendency to varying degrees, most significantly in color tone. By contrast,

**Table 2: Comparison of different intensity allocation strategies in terms of theoretical identity retention and regularization, and experimental similarity and FR performance.**

	Settings	$\mathbb{E}[\cos(\theta)]$	$\mathbb{E}[\sin^2(\theta)]$	CosSim	FR Avg.
(a)	Baseline	/	/	46.1	91.84
	$U(0, 0.75)$	0.784	0.350	42.4	92.68
	$U(0, 1)$	0.637	0.500	38.4	93.21
(b)	Beta(1.6, 1)	0.520	0.639	33.8	93.40
	Beta(2, 1)	0.463	0.703	24.4	/
(c)	$w_{\text{reg}} = 0.1$	0.646	0.526	39.4	93.66
	$w_{\text{reg}} = 1$	0.627	0.565	38.7	93.72

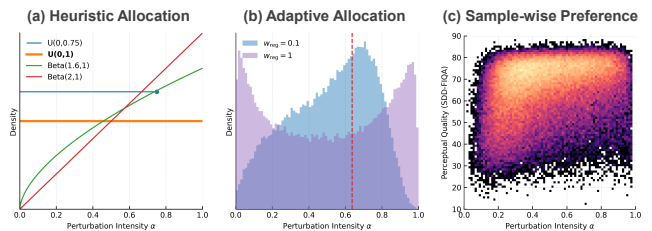


**Figure 8: Allocation of perturbation intensity. (a) Four heuristic distributions for intensity allocation with growing strength. (b) Adaptively learned allocations under different  $w_{\text{reg}}$  differ markedly. (c) Sample-wise preference, where higher-quality samples tend to receive stronger perturbation.**

the average face of SteerFace is much closer to the ground truth, as indicated by its lowest MSE. This suggests that SteerFace effectively mitigates visual tendency, as intended.

### 4.4 Effect of Residue Perturbation

Regarding residue perturbation, we investigate three key questions: *Is it effective? How does its effect relate to intensity allocation? Does it exhibit sample-wise preference adaptively?* We therefore compare different heuristic and adaptive allocations in Tab. 2. For each setting, we report the *theoretical* statistics of identity retention and regularization as per Thm. 1, *i.e.*,  $\mathbb{E}[\cos(\theta)]$  and  $\mathbb{E}[\sin^2(\theta)]$ , as well as the *experimental* cosine similarity and FR performance.

**4.4.1 With vs. Without perturbation.** We compare a baseline generator, trained without perturbation, with the default setting  $w_{\text{reg}} = 1$ . In Tab. 2(a), the baseline shows better identity adherence as identity is not attenuated. However, the default setting outperforms 1.88% in FR performance, which supports the effectiveness of perturbation.

**4.4.2 Heuristic intensity allocation.** We allocate intensity  $\alpha$  from 4 heuristic distributions:  $U(0, 0.75)$ ,  $U(0, 1)$  (the default in Sec. 3.3), Beta(1.6, 1), and Beta(2, 1), shown in Fig. 8(a). As shown in Tab. 2(b), they trade off identity retention and regularization as perturbation strength increases. The corresponding cosine similarity and FR performance vary consistently, indicating that the theoretical trends are also reflected empirically. Overall, downstream FR favors stronger perturbation, with larger  $\mathbb{E}[\sin^2(\theta)]$  yielding higher average accuracy, provided that identity retention remains sufficient.

**Table 3: Generalizability of SteerFace, evaluated across different training datasets and generation pipelines.**

Dataset	Setting	AgeDB	CPLFW	CALFW	Avg.
FFHQ	Baseline	78.53	75.98	86.53	82.16
	$U(0, 1)$	<b>84.08</b>	<b>77.48</b>	<b>88.98</b>	<b>84.54</b>
MS1M	Baseline	89.68	86.65	91.58	91.83
	$U(0, 1)$	<b>90.78</b>	<b>86.88</b>	<b>92.12</b>	<b>92.25</b>
CASIA	UI + Baseline	92.85	87.92	93.25	93.36
	UI + [2]	<b>93.61</b>	<b>88.37</b>	<b>93.50</b>	<b>93.62</b>
	UI + $U(0, 1)$	<u>92.95</u>	<b>89.05</b>	<b>93.52</b>	<b>93.88</b>

Under Beta(2, 1), however, the intra-person similarity becomes too low for training FR model effectively.

**4.4.3 Adaptive intensity allocation.** In Sec. 3.4, the intensity distribution is adaptively learned based on the heuristic  $U(0, 1)$  under the weights  $w_{id}$  and  $w_{reg}$ . Since identity retention  $\mathcal{L}_{id}$  acts as a consistency constraint,  $w_{id}$  is empirically less sensitive. We therefore compare  $w_{reg}$  at 1 (default) and 0.1. Interestingly, Fig. 8(b) shows that their learned distributions differ markedly: with  $w_{reg} = 0.1$ , the distribution favors identity retention and thus concentrates around  $\mathbb{E}_{\alpha \sim U(0,1)}[\cos \theta] \approx 0.637$  (red line); with  $w_{reg} = 1$ , more mass shifts toward the high-intensity tail to strengthen regularization, while the low-intensity tail is also reinforced to preserve identity.

Despite their distinct shapes, Tab. 2 shows that the two distributions yield similar  $\mathbb{E}[\sin^2(\theta)]$  and close FR performance. This supports the analysis in Thm. 1, showing not only that FR performance is governed primarily by regularization strength, but also that it is less sensitive to the exact distributional shape. We further find that both adaptive distributions outperform the heuristic baseline  $U(0, 1)$ , as they maintain comparable  $\mathbb{E}[\cos(\theta)]$  while achieving larger  $\mathbb{E}[\sin^2(\theta)]$ . This explains their FR gains and validates the effectiveness of adaptive perturbation.

**4.4.4 Sample-wise preference.** We empirically find that the learned perturbation intensity correlates with per-image perceptual quality. Specifically, we use SDD-FIQA [40] to assign quality scores to synthetic samples, and plot their correlation with the adaptively allocated intensity. As shown in Fig. 8(c), higher-quality samples tend to be assigned with larger perturbation. We conjecture that such images contain richer high-frequency details, making their residue more biased and therefore in greater need of perturbation. We leave this interesting phenomenon for future investigation.

## 4.5 Generalizability

We further employ SteerFace on two alternative training datasets with substantially different scales: FFHQ [24] with 52K samples and MS-Celeb-1M [19] with 5.2M samples. We also incorporate it into the alternative pipeline of UIFace [33]. Notably, since IDPerturb [2] is by default built on UIFace, we also include it in the comparison. We instantiate SteerFace with the heuristic  $U(0, 1)$  for alignment with IDPerturb; see Sec. 4.6. Results are reported in Tab. 3, with LFW and CFP-FP deferred to the supplementary material.

Overall, SteerFace improves over the baseline in all settings: by 2.38% on FFHQ, 0.42% on MS1M, and 0.52% when integrated into

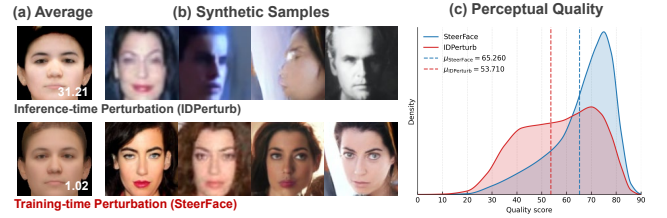


**Figure 9: Inference- vs. training-time perturbation, instantiated as IDPerturb vs. SteerFace. (a) Rendered average faces; IDPerturb remains distributionally biased. (b) Synthetic samples; SteerFace produces higher-quality images. (c) Sample-quality statistics; SteerFace is 11.5% higher in SDD-FIQA.**

UIFace, demonstrating good generalizability. It also outperforms IDPerturb under the latter’s recommended setting. Interestingly, the gains are larger on FFHQ and CASIA (Tab. 2), suggesting that SteerFace may be particularly beneficial when the training dataset is small and thus more prone to bias.

## 4.6 Alternative Perturbation Strategies

We compare SteerFace with two closely related lines of work that also perturb embeddings, as discussed in Sec. 3.3: context dropout [22] and inference-time perturbation [2, 31, 50]. SteerFace is fundamentally different from both and outperforms them.

**4.6.1 Context dropout.** It regularizes model learning by padding embeddings with zero at probability. However, visual tendency can still be learned from the unpadded residues, while identity retention is compromised because dropout perturbs identity and residue components indiscriminately. Experimentally, dropout yields at best 92.32% FR performance, *i.e.*, 1.4% below SteerFace.

**4.6.2 Inference-time perturbation.** It improves data diversity by perturbing embeddings within a local neighborhood on  $\mathbb{S}^{d-1}$ , similarly to Fig. 2(c), to introduce more feature variations. IDPerturb [2] is closest to our method, as it also applies spherical rotation (Eq. (8)), but at inference time. However, such perturbation cannot mitigate visual tendency, as shown in Fig. 9(a), since the bias is inherited during training and only manifests differently at inference time.

Moreover, inference-time perturbation may introduce artifacts by disrupting embedding semantics. In Fig. 9(b), IDPerturb shows failure cases absent in SteerFace. We further assess perceptual quality using SDD-FIQA [40] and plot the score distributions in Fig. 9(c). IDPerturb’s left-shifted distribution indicates statistically degraded sample quality due to such artifacts. For FR performance, since IDPerturb employs a uniform perturbation [2], we instantiate SteerFace with the same heuristic  $U(0, 1)$  for a matched comparison. Table 3 have shown that SteerFace outperforms IDPerturb, suggesting the standalone advantage of training-time perturbation.

See the supplementary material for a more detailed discussion.

## 5 Conclusion

This paper identifies visual tendency as a previously underexplored limitation of synthetic face generation for FR, beyond identity

adherence and data diversity. When conditioned on identity embeddings, diffusion-based generators may unintentionally absorb co-occurring residual visual cues into learned identity semantics, thereby inducing a synthetic-real distribution bias. To address this issue, this paper proposes SteerFace, a simple and efficient training framework that perturbs identity embeddings toward random orthogonal directions on the embedding hypersphere. The perturbation acts as an identity-preserving regularizer and is further combined with an adaptive intensity allocation strategy. Extensive experiments show that SteerFace effectively mitigates visual tendency, improves downstream FR over SOTAs, and generalizes well across different training datasets and generation pipelines.

## References

- [1] Gwangbin Bae, Martin de La Gorce, Tadas Baltrušaitis, Charlie Hewitt, Dong Chen, Julien Valentin, Roberto Cipolla, and Jingjing Shen. 2023. Digiface-1m: 1 million digital face images for face recognition. In *Proceedings of the IEEE/CVF Winter Conference on Applications of Computer Vision*. 3526–3535.
- [2] Fadi Boutros, Eduarda Caldeira, Tahar Chettaoui, and Naser Damer. 2026. IDperturb: Enhancing Variation in Synthetic Face Generation via Angular Perturbation. *arXiv preprint arXiv:2602.18831* (2026).
- [3] Fadi Boutros, Naser Damer, Florian Kirchbuchner, and Arjan Kuijper. 2022. ElasticFace: Elastic Margin Loss for Deep Face Recognition. In *Proceedings of the IEEE/CVF Conference on Computer Vision and Pattern Recognition (CVPR) Workshops*. 1578–1587.
- [4] Fadi Boutros, Jonas Henry Grebe, Arjan Kuijper, and Naser Damer. 2023. Idiff-face: Synthetic-based face recognition through fizzy identity-conditioned diffusion model. In *Proceedings of the IEEE/CVF International Conference on Computer Vision*. 19650–19661.
- [5] Fadi Boutros, Marco Huber, Anh Thi Luu, Patrick Siebke, and Naser Damer. 2024. Sface2: Synthetic-based face recognition with w-space identity-driven sampling. *IEEE Transactions on Biometrics, Behavior, and Identity Science* (2024).
- [6] Fadi Boutros, Marco Huber, Patrick Siebke, Tim Rieber, and Naser Damer. 2022. Sface: Privacy-friendly and accurate face recognition using synthetic data. In *2022 IEEE International Joint Conference on Biometrics (IJCB)*. IEEE, 1–11.
- [7] Fadi Boutros, Marcel Klemm, Meiling Fang, Arjan Kuijper, and Naser Damer. 2023. Exfacegan: Exploring identity directions in gan’s learned latent space for synthetic identity generation. In *2023 IEEE International Joint Conference on Biometrics (IJCB)*. IEEE, 1–10.
- [8] Qiong Cao, Li Shen, Weidi Xie, Omkar M Parkhi, and Andrew Zisserman. 2018. Vggface2: A dataset for recognising faces across pose and age. In *2018 13th IEEE international conference on automatic face & gesture recognition (FG 2018)*. IEEE, 67–74.
- [9] Ivan DeAndres-Tame, Ruben Tolosana, Pietro Melzi, Ruben Vera-Rodriguez, Minchul Kim, Christian Rathgeb, Xiaoming Liu, Luis F. Gomez, Aythami Morales, Julian Fierrez, Javier Ortega-Garcia, Zhizhou Zhong, Yuge Huang, Yuxi Mi, Shouhong Ding, Shuigeng Zhou, et al. 2025. Second FRCSyn-onGoing: Winning solutions and post-challenge analysis to improve face recognition with synthetic data. *Information Fusion* 120 (2025), 103099. doi:10.1016/j.inffus.2025.103099
- [10] Ivan DeAndres-Tame, Ruben Tolosana, Pietro Melzi, Ruben Vera-Rodriguez, Minchul Kim, Christian Rathgeb, Xiaoming Liu, Aythami Morales, Julian Fierrez, Javier Ortega-Garcia, et al. 2024. FrCSyn challenge at cvpr 2024: Face recognition challenge in the era of synthetic data. In *Proceedings of the IEEE/CVF Conference on Computer Vision and Pattern Recognition*. 3173–3183.
- [11] Jiankang Deng, Shiyang Cheng, Niannan Xue, Yuxiang Zhou, and Stefanos Zafeiriou. 2018. Uv-gan: Adversarial facial uv map completion for pose-invariant face recognition. In *Proceedings of the IEEE conference on computer vision and pattern recognition*. 7093–7102.
- [12] Jiankang Deng, Jia Guo, Niannan Xue, and Stefanos Zafeiriou. 2019. Arcface: Additive angular margin loss for deep face recognition. In *Proceedings of the IEEE/CVF conference on computer vision and pattern recognition*. 4690–4699.
- [13] Zheng Ding, Xuaner Zhang, Zhihao Xia, Lars Jebe, Zhuowen Tu, and Xiuming Zhang. 2023. Diffusionrig: Learning personalized priors for facial appearance editing. In *Proceedings of the IEEE/CVF Conference on Computer Vision and Pattern Recognition*. 12736–12746.
- [14] Yao Feng, Haiwen Feng, Michael J Black, and Timo Bolkart. 2021. Learning an animatable detailed 3D face model from in-the-wild images. *ACM Transactions on Graphics (ToG)* 40, 4 (2021), 1–13.
- [15] Rinon Gal, Yuval Alaluf, Yuval Atzmon, Or Patashnik, Amit H Bermano, Gal Chechik, and Daniel Cohen-Or. 2022. An image is worth one word: Personalizing text-to-image generation using textual inversion. *arXiv preprint arXiv:2208.01618* (2022).
- [16] Rinon Gal, Moab Arar, Yuval Atzmon, Amit H Bermano, Gal Chechik, and Daniel Cohen-Or. 2023. Encoder-based domain tuning for fast personalization of text-to-image models. *ACM Transactions on Graphics (TOG)* 42, 4 (2023), 1–13.
- [17] Zhenglin Geng, Chen Cao, and Sergey Tulyakov. 2019. 3d guided fine-grained face manipulation. In *Proceedings of the IEEE/CVF conference on computer vision and pattern recognition*. 9821–9830.
- [18] Jianzhu Guo, Dingyun Zhang, Xiaoqiang Liu, Zhizhou Zhong, Yuan Zhang, Pengfei Wan, and Di Zhang. 2024. Liveportrait: Efficient portrait animation with stitching and retargeting control. *arXiv preprint arXiv:2407.03168* (2024).
- [19] Yandong Guo, Lei Zhang, Yuxiao Hu, Xiaodong He, and Jianfeng Gao. 2016. Ms-celeb-1m: A dataset and benchmark for large-scale face recognition. In *Computer Vision—ECCV 2016: 14th European Conference, Amsterdam, The Netherlands, October 11–14, 2016, Proceedings, Part III 14*. Springer, 87–102.
- [20] Kaiming He, Xiangyu Zhang, Shaoqing Ren, and Jian Sun. 2016. Deep residual learning for image recognition. In *Proceedings of the IEEE conference on computer vision and pattern recognition*. 770–778.
- [21] Jonathan Ho, Ajay Jain, and Pieter Abbeel. 2020. Denoising diffusion probabilistic models. *Advances in neural information processing systems* 33 (2020), 6840–6851.
- [22] Jonathan Ho and Tim Salimans. 2022. Classifier-free diffusion guidance. *arXiv preprint arXiv:2207.12598* (2022).
- [23] Yuge Huang, Yuhang Wang, Ying Tai, Xiaoming Liu, Pengcheng Shen, Shaoxin Li, Jilin Li, and Feiyue Huang. 2020. Curricularface: adaptive curriculum learning loss for deep face recognition. In *proceedings of the IEEE/CVF conference on computer vision and pattern recognition*. 5901–5910.
- [24] Tero Karras, Samuli Laine, and Timo Aila. 2019. A style-based generator architecture for generative adversarial networks. In *Proceedings of the IEEE/CVF conference on computer vision and pattern recognition*. 4401–4410.
- [25] Ira Kemelmacher-Shlizerman, Steven M Seitz, Daniel Miller, and Evan Brossard. 2016. The megaface benchmark: 1 million faces for recognition at scale. In *Proceedings of the IEEE conference on computer vision and pattern recognition*. 4873–4882.
- [26] Minchul Kim, Anil K. Jain, and Xiaoming Liu. 2022. AdaFace: Quality Adaptive Margin for Face Recognition. In *Proceedings of the IEEE/CVF Conference on Computer Vision and Pattern Recognition (CVPR)*. 18750–18759.
- [27] Minchul Kim, Feng Liu, Anil Jain, and Xiaoming Liu. 2023. Dcfac: Synthetic face generation with dual condition diffusion model. In *Proceedings of the IEEE/CVF conference on computer vision and pattern recognition*. 12715–12725.
- [28] Diederik P Kingma. 2014. Adam: A method for stochastic optimization. *arXiv preprint arXiv:1412.6980* (2014).
- [29] Jan Niklas Kolf, Tim Rieber, Jurek Elliesen, Fadi Boutros, Arjan Kuijper, and Naser Damer. 2023. Identity-driven three-player generative adversarial network for synthetic-based face recognition. In *Proceedings of the IEEE/CVF Conference on Computer Vision and Pattern Recognition*. 806–816.
- [30] Gary B. Huang Erik Learned-Miller. 2014. *Labeled Faces in the Wild: Updates and New Reporting Procedures*. Technical Report UM-CS-2014-003. University of Massachusetts, Amherst.
- [31] Shen Li, Jianqing Xu, Jiaying Wu, Miao Xiong, Ailin Deng, Jiazhen Ji, Yuge Huang, Wenjie Feng, Shouhong Ding, and Bryan Hooi. 2024. ID3: Identity-Preserving-yet-Diversified Diffusion Models for Synthetic Face Recognition. *arXiv preprint arXiv:2409.17576* (2024).
- [32] Zhen Li, Mingdeng Cao, Xintao Wang, Zhongang Qi, Ming-Ming Cheng, and Ying Shan. 2024. Photomaker: Customizing realistic human photos via stacked id embedding. In *Proceedings of the IEEE/CVF Conference on Computer Vision and Pattern Recognition*. 8640–8650.
- [33] Xiao Lin, Yuge Huang, Jianqing Xu, Yuxi Mi, Shuigeng Zhou, and Shouhong Ding. 2025. UIFace: Unleashing Inherent Model Capabilities to Enhance Intra-Class Diversity in Synthetic Face Recognition. *arXiv preprint arXiv:2502.19803* (2025).
- [34] Cesar Augusto Fontanillo López et al. 2022. On the legal nature of synthetic data. In *NeurIPS 2022 Workshop on Synthetic Data for Empowering ML Research*.
- [35] Safa C Medin, Bernhard Egger, Anoop Cherian, Ye Wang, Joshua B Tenenbaum, Xiaoming Liu, and Tim K Marks. 2022. MOST-GAN: 3D morphable StyleGAN for disentangled face image manipulation. In *Proceedings of the AAAI conference on artificial intelligence*, Vol. 36. 1962–1971.
- [36] Yuxi Mi, Zhizhou Zhong, Yuge Huang, Jiazhen Ji, Jianqing Xu, Jun Wang, Shaoming Wang, Shouhong Ding, and Shuigeng Zhou. 2024. Privacy-preserving face recognition using trainable feature subtraction. In *Proceedings of the IEEE/CVF Conference on Computer Vision and Pattern Recognition*. 297–307.
- [37] Yuxi Mi, Zhizhou Zhong, Yuge Huang, Qiuyang Yuan, Xuan Zhao, Jianqing Xu, Shouhong Ding, Shaoming Wang, Rizen Guo, and Shuigeng Zhou. 2025. Data synthesis with diverse styles for face recognition via 3dmm-guided diffusion. In *Proceedings of the Computer Vision and Pattern Recognition Conference*. 21203–21214.
- [38] Stylianos Moschoglou, Athanasios Papaioannou, Christos Sagonas, Jiankang Deng, Irene Kotsia, and Stefanos Zafeiriou. 2017. Agedb: the first manually collected, in-the-wild age database. In *proceedings of the IEEE conference on computer vision and pattern recognition workshops*. 51–59.
- [39] Thu Nguyen-Phuoc, Chuan Li, Lucas Theis, Christian Richardt, and Yong-Liang Yang. 2019. Hologan: Unsupervised learning of 3d representations from natural

- images. In *Proceedings of the IEEE/CVF International Conference on Computer Vision*. 7588–7597.
- [40] Fu-Zhao Ou, Xingyu Chen, Ruixin Zhang, Yuge Huang, Shaoxin Li, Jilin Li, Yong Li, Liujuan Cao, and Yuan-Gen Wang. 2021. SDD-FIQA: Unsupervised face image quality assessment with similarity distribution distance. In *Proceedings of the IEEE/CVF conference on computer vision and pattern recognition*. 7670–7679.
- [41] Foivos Paraperas Papanitiou, Alexandros Lattas, Stylianos Moschoglou, Jiankang Deng, Bernhard Kainz, and Stefanos Zafeiriou. 2024. Arc2face: A foundation model of human faces. *arXiv preprint arXiv:2403.11641* (2024).
- [42] Xu Peng, Junwei Zhu, Boyuan Jiang, Ying Tai, Donghao Luo, Jiangning Zhang, Wei Lin, Taisong Jin, Chengjie Wang, and Rongrong Ji. 2024. Portraitbooth: A versatile portrait model for fast identity-preserved personalization. In *Proceedings of the IEEE/CVF Conference on Computer Vision and Pattern Recognition*. 27080–27090.
- [43] Jingtian Piao, Chen Qian, and Hongsheng Li. 2019. Semi-supervised monocular 3D face reconstruction with end-to-end shape-preserved domain transfer. In *Proceedings of the IEEE/CVF international conference on computer vision*. 9398–9407.
- [44] Haibo Qiu, Baosheng Yu, Dihong Gong, Zhifeng Li, Wei Liu, and Dacheng Tao. 2021. Synface: Face recognition with synthetic data. In *Proceedings of the IEEE/CVF International Conference on Computer Vision*. 10880–10890.
- [45] Robin Rombach, Andreas Blattmann, Dominik Lorenz, Patrick Esser, and Björn Ommer. 2022. High-resolution image synthesis with latent diffusion models. In *Proceedings of the IEEE/CVF conference on computer vision and pattern recognition*. 10684–10695.
- [46] Olaf Ronneberger, Philipp Fischer, and Thomas Brox. 2015. U-net: Convolutional networks for biomedical image segmentation. In *Medical image computing and computer-assisted intervention—MICCAI 2015: 18th international conference, Munich, Germany, October 5–9, 2015, proceedings, part III 18*. Springer, 234–241.
- [47] Nataniel Ruiz, Yuanzhen Li, Varun Jampani, Yael Pritch, Michael Rubinstein, and Kfir Aberman. 2023. Dreambooth: Fine tuning text-to-image diffusion models for subject-driven generation. In *Proceedings of the IEEE/CVF conference on computer vision and pattern recognition*. 22500–22510.
- [48] Soumyadip Sengupta, Jun-Cheng Chen, Carlos Castillo, Vishal M Patel, Rama Chellappa, and David W Jacobs. 2016. Frontal to profile face verification in the wild. In *2016 IEEE winter conference on applications of computer vision (WACV)*. IEEE, 1–9.
- [49] Jiaming Song, Chenlin Meng, and Stefano Ermon. 2020. Denoising diffusion implicit models. *arXiv preprint arXiv:2010.02502* (2020).
- [50] Zhonglin Sun, Siyang Song, Ioannis Patras, and Georgios Tzimiropoulos. 2024. Cemiface: Center-based Semi-hard Synthetic Face Generation for Face Recognition. *arXiv preprint arXiv:2409.18876* (2024).
- [51] Dani Valevski, Danny Lumen, Yossi Matias, and Yaniv Leviathan. 2023. Face0: Instantaneously conditioning a text-to-image model on a face. In *SIGGRAPH Asia 2023 Conference Papers*. 1–10.
- [52] Hao Wang, Yitong Wang, Zheng Zhou, Xing Ji, Dihong Gong, Jingchao Zhou, Zhifeng Li, and Wei Liu. 2018. Cosface: Large margin cosine loss for deep face recognition. In *Proceedings of the IEEE conference on computer vision and pattern recognition*. 5265–5274.
- [53] Qinghe Wang, Xu Jia, Xiaomin Li, Taiqing Li, Liqian Ma, Yunzhi Zhuge, and Huchuan Lu. 2024. Stableidentity: Inserting anybody into anywhere at first sight. *arXiv preprint arXiv:2401.15975* (2024).
- [54] Guangxuan Xiao, Tianwei Yin, William T Freeman, Frédo Durand, and Song Han. 2024. Fastcomposer: Tuning-free multi-subject image generation with localized attention. *International Journal of Computer Vision* (2024), 1–20.
- [55] Zunnan Xu, Yachao Zhang, Sicheng Yang, Ronghui Li, and Xiu Li. 2024. Chain of generation: Multi-modal gesture synthesis via cascaded conditional control. In *Proceedings of the AAAI Conference on Artificial Intelligence*, Vol. 38. 6387–6395.
- [56] Dong Yi, Zhen Lei, Shengcai Liao, and Stan Z Li. 2014. Learning face representation from scratch. *arXiv preprint arXiv:1411.7923* (2014).
- [57] Ge Yuan, Xiaodong Cun, Yong Zhang, Maomao Li, Chenyang Qi, Xintao Wang, Ying Shan, and Huicheng Zheng. 2023. Inserting anybody in diffusion models via celeb basis. *arXiv preprint arXiv:2306.00926* (2023).
- [58] Tianyue Zheng and Weihong Deng. 2018. Cross-pose lfw: A database for studying cross-pose face recognition in unconstrained environments. *Beijing University of Posts and Telecommunications, Tech. Rep 5*, 7 (2018), 5.
- [59] Tianyue Zheng, Weihong Deng, and Jiani Hu. 2017. Cross-age lfw: A database for studying cross-age face recognition in unconstrained environments. *arXiv preprint arXiv:1708.08197* (2017).
- [60] Zhizhou Zhong, Yicheng Ji, Zhe Kong, Yiyang Liu, Jiarui Wang, Jiasun Feng, Lupeng Liu, Xiangyi Wang, Yanjia Li, Yuqing She, et al. 2025. Anytalker: Scaling multi-person talking video generation with interactivity refinement. *arXiv preprint arXiv:2511.23475* (2025).
- [61] Zhizhou Zhong, Yuxi Mi, Yuge Huang, Jianqing Xu, Guodong Mu, Shouhong Ding, Jingyun Zhang, Rizen Guo, Yunsheng Wu, and Shuigeng Zhou. 2024. Slerpface: face template protection via spherical linear interpolation. *arXiv preprint arXiv:2407.03043* (2024).
- [62] Yufan Zhou, Ruiyi Zhang, Tong Sun, and Jinhui Xu. 2023. Enhancing detail preservation for customized text-to-image generation: A regularization-free approach. *arXiv preprint arXiv:2305.13579* (2023).
- [63] Zheng Zhu, Guan Huang, Jiankang Deng, Yun Ye, Junjie Huang, Xinze Chen, Jiagang Zhu, Tian Yang, Jiwen Lu, Dalong Du, et al. 2021. Webface260m: A benchmark unveiling the power of million-scale deep face recognition. In *Proceedings of the IEEE/CVF Conference on Computer Vision and Pattern Recognition*. 10492–10502.